

# Nuclear charge densities in spherical and deformed nuclei: towards precise calculations of charge radii

Paul-Gerhard Reinhard<sup>1</sup> and Witold Nazarewicz<sup>2,3</sup>

<sup>1</sup>*Institut für Theoretische Physik, Universität Erlangen, Erlangen, Germany*

<sup>2</sup>*Facility for Rare Isotope Beams, Michigan State University, East Lansing, Michigan 48824, USA*

<sup>3</sup>*Department of Physics and Astronomy, Michigan State University, East Lansing, Michigan 48824, USA*

**Background:** Precise measurements of atomic transitions affected by electron-nucleus hyperfine interactions offer sensitivity to explore basic properties of the atomic nucleus and study fundamental symmetries, including the search for new physics beyond the Standard Model of particle physics. In particular, such measurements, augmented by atomic and nuclear calculations, will enable extraction of the higher-order radial moments of the charge density distribution in spherical and deformed nuclei. The new data impose higher precision requirements on a theoretical description.

**Purpose:** The nuclear charge density is composed of the proton point distribution folded with the nucleonic charge distributions. The latter induce subtle relativistic corrections due to the coupling of nucleon magnetic moments with the nuclear spin-orbit density. Additional corrections come from the effect of center-of-mass projection. We assess the precision of nuclear charge density calculations by studying the behavior of relativistic and center-of-mass motion corrections to the second and fourth charge radial moments. Special attention has been paid to the magnetic spin-orbit density associated with the local variations of the spin-orbit current.

**Methods:** The calculations for semi-magic and open-shell nuclei are performed in the framework of self-consistent mean-field theory using quantified energy density functionals and density-dependent pairing forces. We used the general expression for the spin-orbit form factor that is valid for spherical and deformed nuclei.

**Results:** We studied the impact of various correction terms on the charge radii, fourth radial moments, diffraction radii, and surface thickness of spherical and deformed nuclei. The spin-orbit corrections to charge radial moments and surface thickness show strong shell fluctuations which can make an appreciable effect when aiming at high-precision predictions of isotopic shifts. The inclusion of relativistic and center-of-mass corrections impacts the quality of energy density functionals optimized to charge radii data.

**Conclusions:** To establish reliable constraints on the existence of new forces from isotope shift measurements, precise calculations of nuclear charge densities of deformed nuclei are needed. The proper inclusion of the spin-orbit charge density and other correction terms is essential when aiming at extraction of subtle effects which become particularly visible in isotopic trends. It is also important when developing high-quality nuclear energy density functionals optimized using heterogeneous datasets involving absolute charge radii, differential charge radii, and charge form factor properties deduced from electron scattering data.

## I. INTRODUCTION

High-precision studies of atomic transitions offer complementary information on the structure of atomic nucleus and fundamental symmetries, including hints of new physics beyond the Standard Model of particle physics [1–5]. In particular, precise measurements of transition frequencies allow extraction of tiny variations in the root-mean-square (rms) nuclear charge radii across long isotopic chains of stable and radioactive nuclei [6–12]. This carries the potential to constrain the existence of new forces and hypothetical particles with unprecedented sensitivity [2–4, 6, 13–17]. The theoretical findings have stimulated considerable developments in high-precision experimental techniques [18–21]. The new unprecedented level of precision offers sensitivity not only to explore new physics, but would also provide access to nuclear observables that have so far been elusive, such as the fourth-order charge radial moment  $\langle r^4 \rangle$  [15, 22, 23] that carries information on nuclear surface properties [24, 25].

In order to extract structural information from atomic measurements, it is important for nuclear theory to produce reliable predictions of nuclear charge densities and

currents. Nuclear models usually yield the proton and neutron densities from which the nuclear charge density can be extracted by considering several corrections [26, 27]. The spurious center-of-mass (c.m.) motion is corrected by an unfolding with the width of the centre-of-mass vibrations. The nucleon structure is taken into account by folding with the intrinsic form factor of the free nucleons expressed in terms of the Sachs form factors. The leading part comes from the folding with the nucleonic charge form factors. Moreover, there are the magnetic form factors of the nucleons which contribute to the charge density through the coupling to the nuclear spin-orbit density. The latter contributions are called the spin-orbit terms in the following. Together with the relativistic Darwin-Foldy term, they constitute the relativistic corrections to the charge density [26, 28–32]. (For a recent discussion of the nucleonic corrections see also [33].)

The relativistic corrections are routinely considered in few-body and many-body *ab-initio* nuclear calculations of charge densities and related observables, see, e.g., Refs. [34, 35]. In calculations of charge radii based on the self-consistent mean-field theory [27, 36–38], the pro-

ton and neutron form factor can be expressed in terms of single-particle Hartree-Fock (HF) or Hartree-Fock-Bogoliubov (HFB) densities. The spin-orbit correction is often neglected [5, 25, 39, 40] which is commonly considered reasonable for predictions that do not require high accuracy. Moreover, the majority of calculations with relativistic corrections are carried out in spherical geometry [41–44]; this becomes insufficient when considering long isotopic chains which contain deformed nuclei.

In this work, we take a fresh look at the calculation of nuclear radii under the perspective of the enhanced demands of precision as required by current measurements of nuclear radii. To that end, we apply the self-consistent mean-field theory to study nuclear charge densities and charge radial moments for spherical and deformed nuclei with emphasis on the intrinsic nucleon form factors and the relativistic contributions that are essential for the accuracy required for precision studies. The paper is organized as follows. The definitions of corrections to charge densities and charge radii given in Sec. II. Section III describes the theoretical approach used. This is followed by description of results in Sec. IV. Finally, Sec. V contains the conclusions of our study.

## II. KEY OBSERVABLES

### A. The charge form factor

The nuclear charge density is uniquely related to the nuclear charge form factor  $F_c$ :

$$\rho_c(\mathbf{r}) = \frac{1}{(2\pi)^3} \int d^3q e^{-i\mathbf{q}\cdot\mathbf{r}} F_c(\mathbf{q}). \quad (1)$$

The latter is the quantity measured by electron scattering experiments [28] and used for conveniently including the folding by the intrinsic nucleon form factors and the c.m. motion correction. In the following, we recall the relativistic and non-relativistic expressions for  $F_c$  and briefly discuss the treatment of the c.m. correction.

#### 1. The magnetic contribution to charge density in the relativistic mean-field theory

The relativistic operator for the nuclear charge form factor  $\hat{F}_c$  is the zeroth component of the charge current  $\hat{J}_0$  and reads [26]:

$$\hat{F}_c(\mathbf{q}) \equiv \hat{J}_0(\mathbf{q}) = \sum_{t \in \{p,n\}} f_{1,t}(\mathbf{q}) \hat{\gamma}_0 - f_{2,t}(\mathbf{q}) \frac{\hbar}{2mc} \hat{\boldsymbol{\alpha}} \cdot \mathbf{q}, \quad (2)$$

where  $m$  is the nucleon mass,  $\hat{\boldsymbol{\alpha}}$  is the three-vector of Dirac matrices [45],  $f_{1,t}(\mathbf{q})$  is the intrinsic nucleon charge form factor, and  $f_{2,t}(\mathbf{q})$  is the intrinsic nucleon magnetic form factor. The charge form factor can be written as:

$$F_c(\mathbf{q}) = \sum_{t \in \{p,n\}} \left[ f_{1,t}(\mathbf{q}) F_t(\mathbf{q}) - f_{2,t}(\mathbf{q}) \frac{F_{\text{tens},t}(\mathbf{q}) \hbar}{2mc} \right], \quad (3)$$

where the form factors

$$F_t(\mathbf{q}) = \int d^3r e^{i\mathbf{q}\cdot\mathbf{r}} \rho_t(\mathbf{r}), \quad (4)$$

$$F_{\text{tens},t}(\mathbf{q}) = \int d^3r e^{i\mathbf{q}\cdot\mathbf{r}} \rho_{\text{tens},t}(\mathbf{r}),$$

can be expressed in terms of relativistic densities

$$\rho_t(\mathbf{r}) = \sum_{\alpha \in t} v_\alpha^2 \bar{\psi}_\alpha \hat{\gamma}_0 \psi_\alpha,$$

$$\rho_{\text{tens},t}(\mathbf{r}) = -i \nabla \cdot \sum_{\alpha \in t} v_\alpha^2 \bar{\psi}_\alpha \mathbf{i} \begin{pmatrix} 0 & \boldsymbol{\sigma} \\ \boldsymbol{\sigma} & 0 \end{pmatrix} \psi_\alpha, \quad (5)$$

where the four-component eigenstate of the Dirac equation  $\psi_\alpha$  is the nucleonic single-particle (s.p.) wave function, the  $v_\alpha^2$  are the BCS or HFB canonical pairing occupations, and the tensor density  $\rho_{\text{tens},t}$  together with the nucleon magnetic form factors yield the magnetic contribution to the charge density.

The intrinsic nucleon form factors are usually expressed in terms of the Sachs form factors  $G_E$  and  $G_M$  as

$$f_{1,t}(\mathbf{q}) = \frac{G_{E,t}(\mathbf{q}) + q^2 \mathcal{D} \mu_t G_{M,t}(\mathbf{q})}{1 + q^2 \mathcal{D}}, \quad (6)$$

$$f_{2,t}(\mathbf{q}) = \frac{-G_{E,t}(\mathbf{q}) + \mu_t G_{M,t}(\mathbf{q})}{1 + q^2 \mathcal{D}},$$

where

$$\mathcal{D} = \frac{\hbar^2}{(2mc)^2} \quad (7)$$

and  $\mu_t$  are the magnetic moments of the nucleon:  $\mu_p = 2.79$  and  $\mu_n = -1.91$ .

The above expressions for form factors do not depend on the geometry of the Dirac equation. The explicit spherical-geometry expressions can be found in, e.g., Refs. [42, 43].

#### 2. The magnetic contribution to charge density in non-relativistic mean-field theory

The expression for the form factor in non-relativistic models is obtained by the expansion in powers of  $\mathcal{D} \propto m^{-2}$  up to first order [28]. In this non-relativistic limit, the charge form factor reads [26]:

$$F_c(\mathbf{q}) = \sum_{t \in \{p,n\}} \left[ G_{E,t}(\mathbf{q}) \left( 1 - \frac{1}{2} q^2 \mathcal{D} \right) F_t(\mathbf{q}) - \mathcal{D} [2\mu_t G_M(\mathbf{q}) - G_{E,t}(\mathbf{q})] F_{\ell s,t}(\mathbf{q}) \right]. \quad (8)$$

The form factors

$$F_t(\mathbf{q}) = \int d^3r e^{i\mathbf{q}\cdot\mathbf{r}} \rho_t(\mathbf{r}), \quad (9)$$

$$F_{\ell s,t}(\mathbf{q}) = \int d^3r e^{i\mathbf{q}\cdot\mathbf{r}} \nabla \cdot \mathbf{J}_t(\mathbf{r})$$

are given in terms of the local particle densities  $\rho_t(\mathbf{r})$  and spin-orbit currents  $\mathbf{J}_t(\mathbf{r})$ :

$$\begin{aligned}\rho_t(\mathbf{r}) &= \sum_{\alpha} v_{\alpha}^2 |\varphi_{t\alpha}(\mathbf{r})|^2, \\ \mathbf{J}_t(\mathbf{r}) &= i \sum_{\alpha} v_{\alpha}^2 \varphi_{t\alpha}^*(\mathbf{r}) (\boldsymbol{\sigma} \times \nabla) \varphi_{t\alpha}(\mathbf{r}),\end{aligned}\quad (10)$$

with  $\varphi_{t\alpha}(\mathbf{r})$  being the canonical HFB (or BCS) wave functions and  $v_{\alpha}^2$  the corresponding pairing occupation coefficients. Note that the above derivation does not make assumptions about spatial symmetries. Consequently, the expressions can be applied in 3D HFB codes as well as in 2D axial or 1D spherical HFB calculations.

There is a subtle difference in the interpretation of the relativistic and non-relativistic expressions. In the relativistic form factor, the magnetic contributions are associated simply with the tensor density. In the non-relativistic case, this becomes the spin-orbit density and it turns out to be of the same order  $\mathcal{D}$  as the relativistic Darwin term  $G_E \mathcal{D}$ . It is customary, to consider the purely electric contribution  $G_{E,t} F_t$  as the leading term and everything else as relativistic correction.

### 3. The center-of-mass contribution to charge density

There are several ways to describe the c.m. correction formally [46–48]. For calculations in coordinate-space basis, as in this work, the most appropriate is the approximate projection technique [46]. In the second-order Gaussian overlap approximation, the projected point-proton form factor can be written as:

$$F_p^{\text{proj}}(\mathbf{q}) = F_p(\mathbf{q}) \exp\left(\frac{3}{8\langle\Phi|\hat{\mathbf{P}}^2|\Phi\rangle} \mathbf{q}^2\right), \quad (11)$$

where  $|\Phi\rangle$  is the BCS or HFB state and  $\mathbf{P}$  is the c.m. momentum. This expression is analogous to that obtained in the harmonic oscillator expansion [47, 48].

The quality of the approximation (11) has been examined in Ref. [46]. It was concluded that the bulk nuclear properties as the diffraction radius and surface thickness are more robust and show little difference between approximate and exact projection. Noteworthy effects appear only for light nuclei up to Ca, reaching to typically 0.0004 fm uncertainty for Ca.

### B. The charge radius

The squared charge radius is obtained from the charge form factor  $F_c(\mathbf{q})$  as

$$\langle r_c^2 \rangle = - \frac{\nabla^2 F_c(\mathbf{q})|_{q=0}}{F_c(0)}. \quad (12)$$

For the reflection-symmetric nuclei, all form factors  $F(\mathbf{q})$  in Eq. (8) fulfill the condition:  $\nabla F(\mathbf{q}) = 0$ . The product rule with  $\nabla^2$  then yields only terms with zeroth or second derivative. We abbreviate  $\nabla^2 f|_{q=0} = f''$  for each factor in the form factor and insert the values in zeroth order  $G_{E,p}(0) = 1$ ,  $G_{E,n}(0) = 0$ ,  $G_M(0) = 1$ ,  $F_p(0) = Z$ ,  $F_n(0) = N$ , and  $F_{\ell s,t}(q)(0) = 0$ . This yields at  $q = 0$ :

$$F_c = Z, \quad (13)$$

$$\begin{aligned}F_c'' &= F_p'' + ZG_{E,p}'' - 3Z\mathcal{D} + NG_{E,n}'' \\ &\quad - (2\mu_p - 1)\mathcal{D}F_{\ell s,p}'' - 2\mu_n\mathcal{D}F_{\ell s,n}''.\end{aligned}\quad (14)$$

The second derivatives can be written as

$$F_p'' = \int d^3r r^2 \rho_p(\mathbf{r}) \equiv Z \langle r^2 \rangle_{pp}, \quad (15)$$

$$F_{\ell s,t}'' = \int d^3r r^2 \nabla \cdot \mathbf{J}_t(\mathbf{r}) \quad (16)$$

and similarly  $G_{E,p}'' = \langle r^2 \rangle_p^{(\text{intr})}$ ,  $G_{E,n}'' = \langle r^2 \rangle_n^{(\text{intr})}$ . In the above expression,  $\langle r^2 \rangle_{pp}$  indicates the point-proton radius as it emerges directly from the mean-field calculation. The quantity  $F_{\ell s,t}''$  can alternatively be written as:

$$F_{\ell s,t}'' = -2\langle \hat{\boldsymbol{\sigma}} \cdot \hat{\boldsymbol{\ell}} \rangle_t. \quad (17)$$

which adds a physical interpretation. In practice, we evaluate  $F_{\ell s,t}''$  in terms of Eq. (16) because the local spin-orbit current  $\mathbf{J}_t$  is already provided by the HFB calculations.

By combining all contributions, we obtain the expression or the average squared charge radius:

$$\langle r_c^2 \rangle = \langle r_{pp}^2 \rangle + \langle r_p^2 \rangle^{(\text{intr})} + \frac{N}{Z} \langle r_n^2 \rangle^{(\text{intr})} + \langle r^2 \rangle^{(\text{rel})}, \quad (18)$$

where

$$\langle r^2 \rangle^{(\text{rel})} = 3\mathcal{D} + (\mu_p - \frac{1}{2}) \frac{4}{Z} \mathcal{D} \langle \hat{\boldsymbol{\sigma}} \cdot \hat{\boldsymbol{\ell}} \rangle_p + \mu_n \frac{4}{Z} \mathcal{D} \langle \hat{\boldsymbol{\sigma}} \cdot \hat{\boldsymbol{\ell}} \rangle_n \quad (19)$$

is the relativistic contribution to the charge radius. As discussed above, it consists of the Darwin-Foldy (DF) term  $3\mathcal{D}$  and the spin-orbit corrections.

The form of the spin-orbit terms in Eq. (16) that involves  $\nabla \cdot \mathbf{J}$  is valid for arbitrary mean-field geometry. The second form (17), involving  $\langle \hat{\boldsymbol{\sigma}} \cdot \hat{\boldsymbol{\ell}} \rangle_t$ , is particularly useful if the spherical geometry is imposed. In this case, the expectation value of the spin-orbit term becomes independent of the radial profile of the wave functions and the expression reduces (for each nucleon type) to  $\langle \hat{\boldsymbol{\sigma}} \cdot \hat{\boldsymbol{\ell}} \rangle = \sum_{\alpha} v_{\alpha}^2 (\sigma l)_{\alpha}$  where  $(\sigma l)_{\alpha} = j_{\alpha}(j_{\alpha} + 1) - l_{\alpha}(l_{\alpha} + 1) - \frac{3}{4}$ , which is  $l_{\alpha}$  for  $j_{\alpha} = l_{\alpha} + 1/2$  and  $-(l_{\alpha} + 1)$  for  $j_{\alpha} = l_{\alpha} - 1/2$ . It is immediately seen that if both sub-shells of the spin-orbit doublet are occupied with the same weight, their contribution to the  $\ell s$  term in (18) vanishes (spin-saturated case). The maximal spin-orbit contribution is attained when the lower-energy member of the spin-orbit doublet is fully occupied and the upper-energy member with  $j = \ell - 1/2$  is not [26].

### III. COMPUTATIONAL FRAMEWORK

The examples presented here were computed with non-relativistic nuclear density-functional theory (DFT) using the well known Skyrme energy-density functional, for a detailed review see [37]. In our applications, we employ the Skyrme parametrization SV-bas from Ref. [49] which has been optimized to a large experimental calibration dataset including information on several exotic nuclei. This is appropriate for the present study, which covers long isotopic and isotonic chains. We have repeated calculations presented in this work with other Skyrme parametrizations and obtained results that are very similar to those with SV-bas. We also employed the Fayans functional  $F_Y(\Delta r, \text{HFB})$  [9, 50], which uses the optimization dataset of SV-bas and adds to it a crucial new input consisting of differential charge radii in the calcium chain.

To cover deformed nuclei, we use the recently published code `SkyAx` which allows for deformed axially symmetric shapes [51]. A word is in order about the treatment of pairing. The code `SkyAx` implements pairing at the BCS level using a soft cutoff in pairing space with the cutoff profile as used in Ref. [52]

$$w_\alpha = [1 + \exp((\varepsilon_\alpha - (\epsilon_{F,q_\alpha} + \epsilon_{\text{cut}}))/\Delta\epsilon)]^{-1} \quad (20)$$

where  $\varepsilon_\alpha$  are the s.p. energies,  $\epsilon_{\text{cut}}$  marks the cutoff band, and  $\Delta\epsilon = \epsilon_{\text{cut}}/10$  is its width. We use a dynamical setting of the pairing band where  $\epsilon_{\text{cut}}$  is adjusted such that a fixed number of nucleons  $N_q + \eta_{\text{cut}} N_q^{2/3}$  is included in the sum  $\sum_{\alpha \in q} w_\alpha$  [53], here with  $\eta_{\text{cut}} = 1.65$  for SV-bas (as in Ref. [49]) and  $\eta_{\text{cut}} = 5$  for  $F_Y(\Delta r, \text{HFB})$  as in [50].

It is to be noted that mere BCS is not always appropriate for nuclei at the edges of stability [9, 54, 55], for which one should use, in principle, the full HFB framework. In this study, however, we limit the selection generally to nuclei whose proton and neutron Fermi energies are sufficiently bound so the unphysical particle gas effects are avoided.

The intrinsic form factors of the nucleons were computed as in Ref. [38] with the Sachs form factors taken from Refs. [56, 57]. We wish to emphasize that we do not use Eq. (18) to estimate charge radii but rather compute numerically the radial moments (as well as other observables directly from the charge density and charge form factor) by the folding the point charge distribution with the intrinsic nucleon form factors. In this way, all contributions to the charge density are automatically included. In this work, we consider subtle effects stemming from the relativistic corrections that place great demands on the accuracy of underlying calculations. In order to compute charge radii with precision better than 0.001 fm, the calculations were carried out with enhanced demands on grid spacing, box size, Fourier transform, and HF+BCS termination criteria.

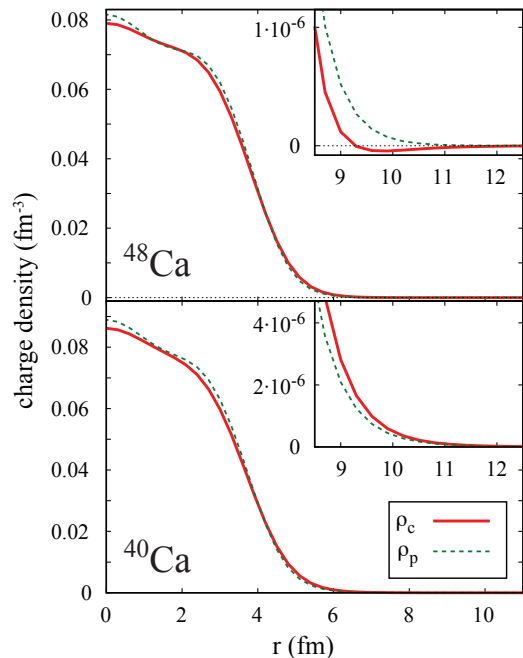


FIG. 1. Comparison of charge and proton densities for  $^{40}\text{Ca}$  and  $^{48}\text{Ca}$  computed with SV-bas. The density dependence at large distances is shown in the insets.

### IV. RESULTS

We shall begin from a pedagogical Fig. 1 showing the charge density (1) predicted with SV-bas for  $^{40}\text{Ca}$  and  $^{48}\text{Ca}$ . It is seen that at large distances the neutron charge distribution and, to a lesser extent, the neutron spin-orbit density produce a negative contribution to the charge density in  $^{48}\text{Ca}$ , while the effect of correction terms to the proton density in  $^{40}\text{Ca}$  is less pronounced. The resulting negative contribution to the charge radius helps bringing the charge radius of  $^{48}\text{Ca}$  very close to the value in  $^{40}\text{Ca}$  [6, 34, 42, 43, 58], see discussion around Table I below..

Figure 2 shows the predicted rms proton and charge radii along selected isotopic chains which cover spherical and deformed nuclei. The nucleonic and relativistic corrections are of the order of 0.05 fm. This suggests that in applications where one aims merely at a global description of radii one may use the approximate relation [26]

$$\langle r_c^2 \rangle \approx \langle r_{pp}^2 \rangle + \langle r_p^2 \rangle^{(\text{intr})} + (N/Z) \langle r_n^2 \rangle^{(\text{intr})} \quad (21)$$

with the constant proton and neutron charge radii:  $\langle r_p \rangle^{(\text{intr})} = 0.848 \text{ fm}$  [59] and  $\langle r_n^2 \rangle^{(\text{intr})} = -0.1161 \text{ fm}^2$  [60], which is the radius correction (18) without the relativistic term  $\langle r^2 \rangle^{(\text{rel})}$ . (Note that the previous implementation of the proton form factor in Refs. [38, 56, 57] implies the older value of the proton radius  $\langle r_p \rangle^{(\text{intr})} = 0.854 \text{ fm}$  which amounts to a constant reduction of about 0.001 fm, with no effect on trends.)

Figure 3 shows the c.m. correction to the charge radii of Ca isotopes. It is seen that the c.m. correction varies

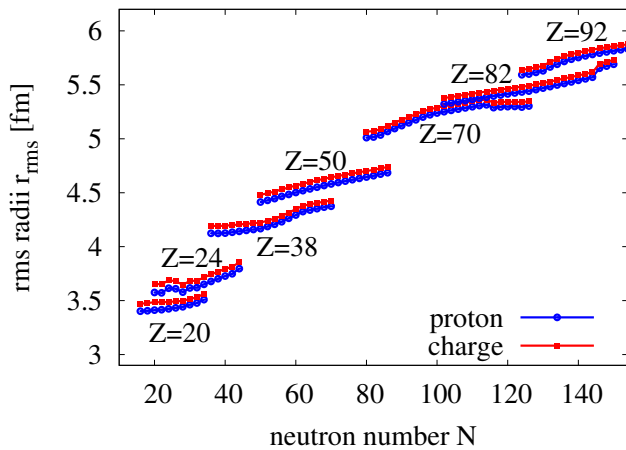


FIG. 2. The rms point-proton (blue) and charge radii (red) for isotopic chains of magic (Ca, Sn, Pb) and open-shell (Cr, Sr, Yb, U) nuclei computed with SV-bas.

very smoothly with neutron number. Such a smooth trend holds also for the possible systematic error from approximate c.m. projection. Consequently, this already small error becomes reduced for differential radii. We can thus conclude that small errors on the charge radii due to the c.m. treatment have negligible consequences for differential radii, for which high precision is required.

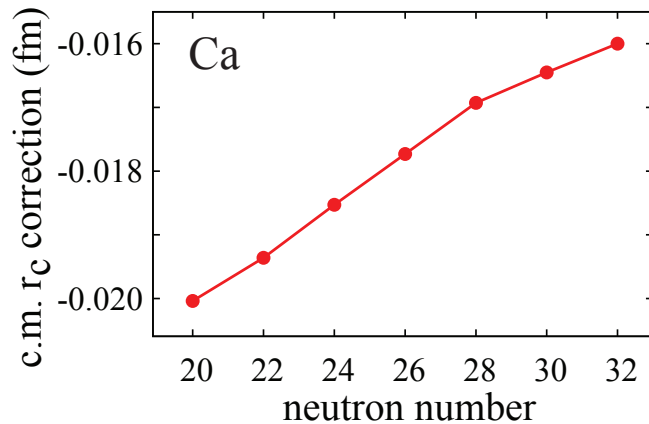


FIG. 3. The c.m. correction to the charge radii of Ca isotopes computed with SV-min.

On the other hand, the relativistic correction must be included in precision calculations (which aims at average uncertainties as low as 0.015 fm) and studies of small local variations of charge radii such as the discontinuities across shell closures, which requires accuracy on charge radius prediction well below 0.01 fm [10]. To quantify this point, Table I shows the impact of the spin-orbit contribution to the charge form factor on the results of the nuclear energy functional parametrizations SV-bas and Fy( $\Delta r$ ,HFB) optimized to large experimental datasets including form-factor information. The r.m.s.

TABLE I. Properties of charge density computed with and without spin-orbit contribution to the charge form factor for two energy density functionals: SV-bas and Fy( $\Delta r$ ,HFB). The rms deviations from data for the diffraction radius, surface thickness, and charge radius (all in  $10^{-3}$  fm) are  $\Delta R_c$ ,  $\Delta\sigma_c$ , and  $\Delta r_c$ , respectively. We compute  $R_c$  and  $\sigma_c$  consistently from the charge form factor  $F_c$  as discussed in [51]. The differential mean-square charge radii for the Ca isotopes are defined in the usual way:  $\delta\langle r^2 \rangle^{A',A} = \langle r^2 \rangle^{(A)\text{Ca}} - \langle r^2 \rangle^{(A')\text{Ca}}$ . Their experimental values are  $\delta\langle r^2 \rangle^{40,48} = 0.007 \text{ fm}^2$  and  $\delta\langle r^2 \rangle^{44,48} = 0.308 \text{ fm}^2$ . The  $\chi^2$  is the overall quality measure for the fit, see [49].

|                                     | SV-bas |  | Fy( $\Delta r$ ,HFB) |  |
|-------------------------------------|--------|--|----------------------|--|
|                                     | full   | no $\langle \hat{\sigma} \cdot \hat{\ell} \rangle_t$ | full                 | no $\langle \hat{\sigma} \cdot \hat{\ell} \rangle_t$ |
| $\Delta R_c$                        | 34     | 33   | 29                   | 27   |
| $\Delta\sigma_c$                    | 26     | 29   | 17                   | 20   |
| $\Delta r_c$                        | 13     | 15   | 17                   | 16   |
| $\delta\langle r^2 \rangle^{40,48}$ | 0.109  | 0.205  | 0.010                | 0.112  |
| $\delta\langle r^2 \rangle^{44,48}$ | -0.083 | -0.128   | 0.294                | 0.235  |
| $\chi^2$                            | 56.9   | 62.6   | 65.1                 | 125.8  |

deviations from experiment for the robust global observables, namely the diffraction radius, surface thickness, and charge radius, depend, at first glance, weakly on the spin-orbit correction. But note that the changes amount to 3–15%, which has a visible impact on the overall quality of the fit. This is already the case for SV-bas, for which isotopic shifts have not included in the optimization dataset. The differential mean-square charge radii  $\delta\langle r^2 \rangle^{A',A}$  are more refined observables and they react quite dramatically. This becomes apparent in the huge change of  $\chi^2$  for Fy(Dr,HFB) because this parametrization includes the isotopic shifts in the fit data. We conclude that a description of isotope shifts without the spin-orbit correction is grossly misleading.

To show the effect of spin-orbit correction on charge radii in detail, Fig. 4 displays the difference  $\langle r_c^2 \rangle - \langle r_{pp}^2 \rangle$  for the isotopic chains of Fig. 2. For each chain, the results without the spin-orbit term exhibit a smooth decrease with neutron number that is consistent with the behavior of the intrinsic neutron charge distribution term in Eq. (21). As expected, the spin-orbit contribution strongly fluctuates with  $N$ . In the regions corresponding to the gradual occupation of high- $j$  unique-parity shells the spin-orbit correction rapidly decreases due to the negative value of  $\mu_n$ . The local increasing trends can be associated with the gradual occupation of the upper spin-orbit partner.

The most dramatic local variation of relativistic contributions is predicted between  $^{40}\text{Ca}$  and  $^{52}\text{Ca}$  (due to the population of  $1f_{7/2}$  and  $2p_{3/2}$  neutron shells) and in the Sr chain around  $N = 50$  (due to the population of  $1g_{9/2}$  and  $2d_{5/2}$  neutron shells). In heavy nuclei the variations tend to be more gradual due to the fragmentation of the spin-orbit strength and the smoothing effect of pairing.

Figure 5 illustrates the behavior of  $\langle r_c^2 \rangle - \langle r_{pp}^2 \rangle$  along

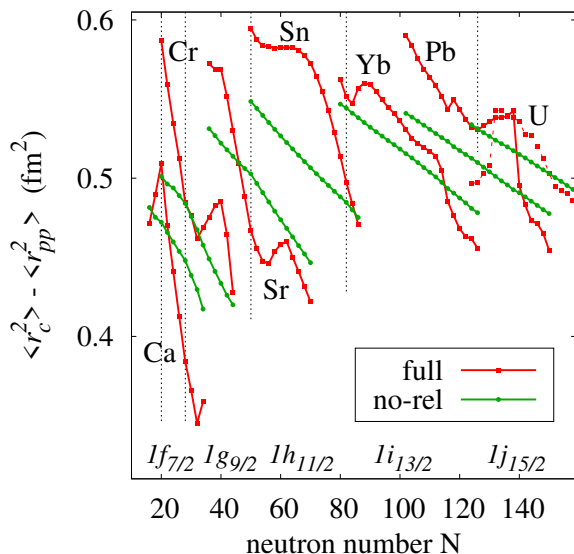


FIG. 4. The difference  $\langle r_c^2 \rangle - \langle r_{pp}^2 \rangle$  for several isotopic chains. For comparison, the results without relativistic contribution (19) are shown. Magic numbers are indicated by vertical dashed lines. Positions of unique-parity shells are marked.

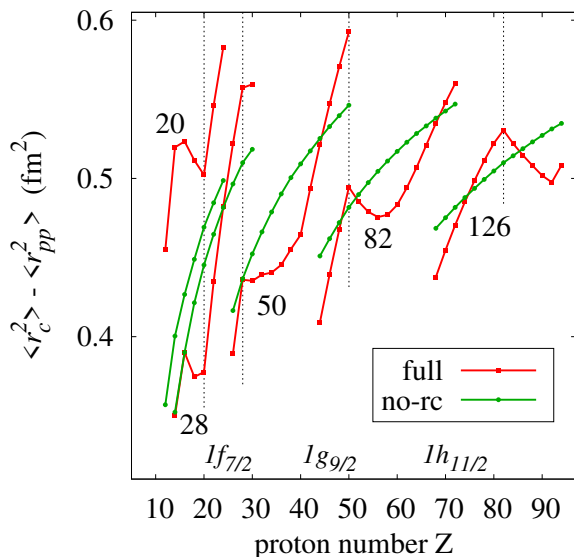


FIG. 5. Similar to Fig. 4 but for several isotonic chains of semi-magic nuclei.

the isotonic chains of semi-magic nuclei. Here, due to the positive value of  $(\mu_p - 1/2)$ , the spin-orbit contribution increases with  $Z$  in the regions in which high- $j$  shell are occupied. The largest shell effect is predicted for  $N = 28$ ; it is seen in the rapid rise of the spin-orbit correction between  $^{48}\text{Ca}$  and  $^{56}\text{Ni}$ . Appreciable kinks in  $\langle r_c^2 \rangle$  are expected at  $Z = 50$  and  $82$  where the  $j = \ell + 1/2$  shells close up and the  $j = \ell - 1/2$  shells become occupied.

To illustrate the impact of deformation effects, Fig. 6 shows the corrections to the difference  $\langle r_c^2 \rangle - \langle r_{pp}^2 \rangle$  along the Yb chain. We note that the deformed Yb isotopes

are of particular interest in the context of ongoing experimental searches of new physics [21]. The intrinsic proton contribution, DF, and c.m. terms do not vary with  $N$ . The intrinsic neutron contribution shows the trivial linear  $N/Z$  dependence. Note that in the deformed region the spin-orbit contributions change gradually as the single-particle spin-orbit strength becomes highly fragmented by deformation and pairing. The prolate-to-oblate shape transitions seen in the extremely proton-rich and extremely neutron-rich isotopes result in noticeable variations of spin-orbit contributions.

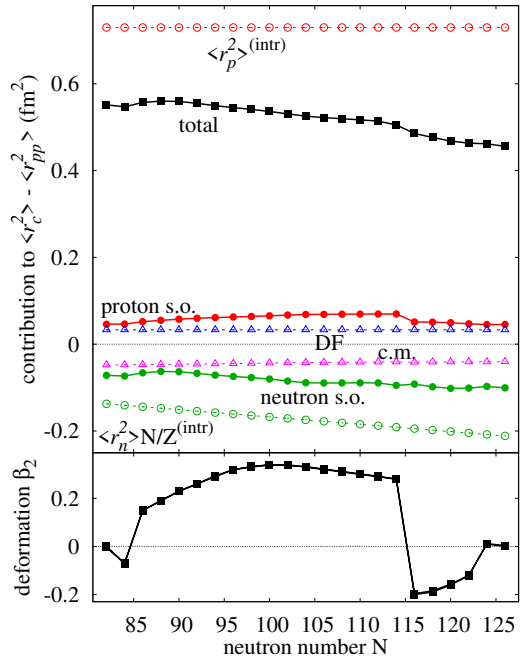


FIG. 6. Top: various corrections to  $\langle r_c^2 \rangle - \langle r_{pp}^2 \rangle$  along the chain of Yb isotopes. Bottom: dimensionless quadrupole shape deformation parameter  $\beta_2 = 4\pi\langle Q_{20} \rangle / (5AR^2)$ , where  $Q_{20}$  is the mass quadrupole moment and  $R_c$  the diffraction radius.

As demonstrated recently [24], the fourth radial moment  $\langle r^4 \rangle$  can be directly related to the surface thickness  $\sigma$  of nuclear density. (See also discussion in Ref. [43].) Precise knowledge of  $\langle r^4 \rangle$  is essential to establish reliable constraints on new physics. The fourth radial moment  $\langle r^4 \rangle$  is computed from the charge density as obtained from  $F_c$  by the inverse Fourier transform (which we find the simplest and most robust procedure). In order to demonstrate the sensitivity of  $\langle r_c^4 \rangle$  and bulk nuclear surface properties on the spin-orbit charge densities Figs. 7 and 8 illustrate the impact of relativistic corrections on  $\langle r^4 \rangle$ , surface thickness  $\sigma$ , and diffraction radii  $R_c$  (see Ref. [24] for definitions). It is seen that the shell fluctuations of relativistic corrections to these quantities are appreciable for  $\langle r^4 \rangle$  and  $\sigma_c$  while  $R_c$  is less sensitive.

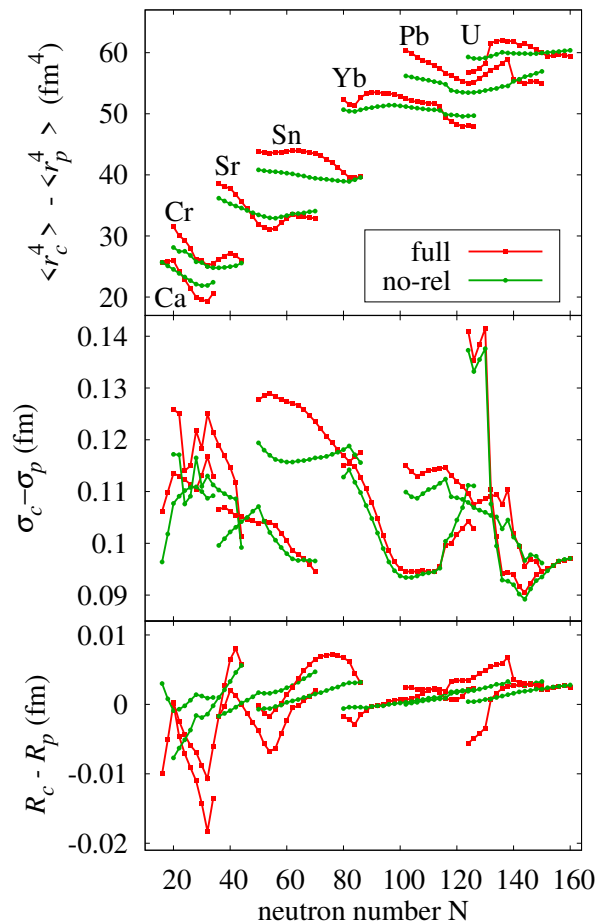


FIG. 7. The corrections to the fourth radial moment  $\langle r^4 \rangle$ , surface thickness  $\sigma$ , and diffraction radius  $R_c$  along several isotopic chains. For comparison, the results without relativistic contribution are also shown.

## V. CONCLUSIONS

In this study, we investigated the impact of nucleonic corrections to the nuclear charge density and charge radial moments that are important in the context of precise measurements of isotopic shifts. The calculations were performed for spherical and deformed nuclei in the framework of self-consistent mean-field theory using quantified nuclear energy density functionals and density-dependent pairing forces. We used the general expression for the spin-orbit form factor that is valid for deformed nuclei. The main conclusions and results of our study can be summarized as follows:

- (i) The nucleonic corrections are of the order of 0.05 fm. While the electric nucleonic corrections to charge radii do not depend on shell structure and can be simply accounted for, the magnetic spin-orbit corrections strongly vary with particle number and require careful modelling. These corrections can amount up to 0.01 fm and need to be accounted for in precision studies aiming at extrac-

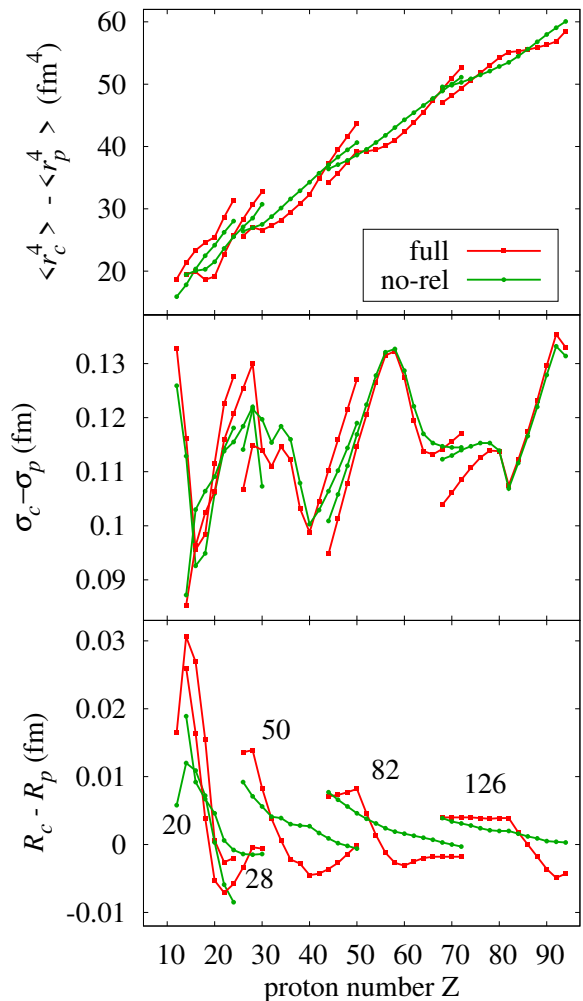


FIG. 8. Similar to Fig. 7 but for several isotonic chains of semi-magic nuclei.

tion of tiny effects due to new physics from differential radii.

- (ii) Spin-orbit corrections, with their pronounced shell effects, play a role during the optimization of nuclear energy density functionals to the datasets involving charge radii. On the other hand, the uncertainty on the charge radii due to the c.m. treatment has negligible consequences for differential radii, provided that the underlying EDF has been optimized to datasets including charge radii.
- (iii) The discontinuities in charge radii across shell closures results in kinks, which are well below 0.01 fm, [10]. Since some of the nuclei of interest are open-shell systems [61], contributions from deformed spin-orbit densities can be appreciable.
- (iv) Deformation and pairing give rise to the fragmentation of the spin-orbit strength. This results in a smoothing of the spin-orbit correction to charge

radii. To estimate this fragmentation for heavy nuclei, the deformed formalism laid out in this work can be applied.

- (v) It will be interesting to investigate experimentally the charge radii along the isotonic chains of semi-magic nuclei. Here, our calculations predict a large shell effect for  $N = 28$  that is characterized in the rapid rise of the spin-orbit correction between  $^{48}\text{Ca}$  and  $^{56}\text{Ni}$ . Also, appreciable kinks in  $\langle r_c^2 \rangle$  are expected at  $Z = 50$  and  $82$  due to the closing of pro-

ton  $1g_{9/2}$  and  $1h_{11/2}$  intruder shells and filling the  $1g_{7/2}$  and  $1h_{9/2}$  spin-orbit partner shells

## ACKNOWLEDGMENTS

This material is based upon work supported by the U.S. Department of Energy, Office of Science, Office of Nuclear Physics under award numbers DE-SC0013365 and DE-SC0018083 (NUCLEI SciDAC-4 collaboration).

- 
- [1] M. S. Safronova, D. Budker, D. DeMille, D. F. J. Kimball, A. Derevianko, and C. W. Clark, “Search for new physics with atoms and molecules,” *Rev. Mod. Phys.* **90**, 025008 (2018).
- [2] J. C. Berengut, D. Budker, C. Delaunay, V. V. Flambaum, C. Frugiuele, E. Fuchs, C. Grojean, R. Harnik, R. Ozeri, G. Perez, and Y. Soreq, “Probing new long-range interactions by isotope shift spectroscopy,” *Phys. Rev. Lett.* **120**, 091801 (2018).
- [3] Y. V. Stadnik, “Probing Long-Range Neutrino-Mediated Forces with Atomic and Nuclear Spectroscopy,” *Phys. Rev. Lett.* **120**, 223202 (2018).
- [4] C. Delaunay, C. Frugiuele, E. Fuchs, and Y. Soreq, “Probing new spin-independent interactions through precision spectroscopy in atoms with few electrons,” *Phys. Rev. D* **96**, 115002 (2017).
- [5] A. V. Viatkina, D. Antypas, M. G. Kozlov, D. Budker, and V. V. Flambaum, “Dependence of atomic parity-violation effects on neutron skins and new physics,” *Phys. Rev. C* **100**, 034318 (2019).
- [6] R. F. Garcia Ruiz, M. L. Bissell, K. Blaum, A. Ekström, N. Frömmgen, G. Hagen, M. Hammen, K. Hebel, J. D. Holt, G. R. Jansen, *et al.*, “Unexpectedly large charge radii of neutron-rich calcium isotopes,” *Nature Phys.* **12**, 594–598 (2016).
- [7] P. Campbell, I. Moore, and M. Pearson, “Laser spectroscopy for nuclear structure physics,” *Prog. Part. Nucl. Phys.* **86**, 127–180 (2016).
- [8] M. Hammen, W. Nörtershäuser, D. L. Balabanski, M. L. Bissell, K. Blaum, I. Budincevic, B. Cheal, K. T. Flanagan, N. Frömmgen, G. Georgiev, *et al.*, “From Calcium to Cadmium: Testing the Pairing Functional through Charge Radii Measurements of  $^{100-130}\text{Cd}$ ,” *Phys. Rev. Lett.* **121**, 102501 (2018).
- [9] A. J. Miller, K. Minamisono, A. Klose, D. Garand, C. Kujawa, J. D. Lantis, Y. Liu, B. Maaß, P. F. Mantica, W. Nazarewicz, *et al.*, “Proton superfluidity and charge radii in proton-rich calcium isotopes,” *Nature Phys.* **15**, 432–436 (2019).
- [10] C. Gorges, L. V. Rodríguez, D. L. Balabanski, M. L. Bissell, K. Blaum, B. Cheal, R. F. Garcia Ruiz, G. Georgiev, W. Gins, H. Heylen, A. Kanellakopoulos, S. Kaufmann, M. Kowalska, V. Lagaki, S. Lechner, B. Maaß, S. Malbrunot-Ettenauer, W. Nazarewicz, R. Neugart, G. Neyens, W. Nörtershäuser, P.-G. Reinhard, S. Sailer, R. Sánchez, S. Schmidt, L. Wehner, C. Wraith, L. Xie, Z. Y. Xu, X. F. Yang, and D. T. Yordanov, “Laser spectroscopy of neutron-rich tin isotopes: A discontinuity in charge radii across the  $N = 82$  shell closure,” *Phys. Rev. Lett.* **122**, 192502 (2019).
- [11] R. P. de Groote, J. Billowes, C. L. Binnersley, M. L. Bissell, T. E. Cocolios, T. Day Goodacre, G. J. Farooq-Smith, D. V. Fedorov, K. T. Flanagan, S. Franchoo, R. F. Garcia Ruiz, W. Gins, J. D. Holt, Á. Kossorús, K. M. Lynch, T. Miyagi, W. Nazarewicz, G. Neyens, P. G. Reinhard, S. Rothe, H. H. Stroke, A. R. Vernon, K. D. A. Wendt, S. G. Wilkins, Z. Y. Xu, and X. F. Yang, “Measurement and microscopic description of odd-even staggering of charge radii of exotic copper isotopes,” *Nat. Phys.* **16**, 620–624 (2020).
- [12] D. T. Yordanov, L. V. Rodríguez, D. L. Balabanski, J. Bieroń, M. L. Bissell, K. Blaum, B. Cheal, J. Ekman, G. Gaigalas, R. F. Garcia Ruiz, G. Georgiev, W. Gins, M. R. Godefroid, C. Gorges, Z. Harman, H. Heylen, P. Jönsson, A. Kanellakopoulos, S. Kaufmann, C. H. Keitel, V. Lagaki, S. Lechner, B. Maaß, S. Malbrunot-Ettenauer, W. Nazarewicz, R. Neugart, G. Neyens, W. Nörtershäuser, N. S. Oreshkina, A. Pappouli, P. Pyykkö, P.-G. Reinhard, S. Sailer, R. Sánchez, S. Schiffmann, S. Schmidt, L. Wehner, C. Wraith, L. Xie, Z. Xu, and X. Yang, “Structural trends in atomic nuclei from laser spectroscopy of tin,” *Commun. Phys.* **3**, 107 (2020).
- [13] C. Delaunay, R. Ozeri, G. Perez, and Y. Soreq, “Probing atomic Higgs-like forces at the precision frontier,” *Phys. Rev. D* **96**, 93001 (2017).
- [14] C. Frugiuele, E. Fuchs, G. Perez, and M. Schlaffer, “Constraining new physics models with isotope shift spectroscopy,” *Phys. Rev. D* **96**, 015011 (2017).
- [15] V. V. Flambaum, A. J. Geddes, and A. V. Viatkina, “Isotope shift, nonlinearity of King plots, and the search for new particles,” *Phys. Rev. A* **97**, 032510 (2018).
- [16] K. Mikami, M. Tanaka, and Y. Yamamoto, “Probing new intra-atomic force with isotope shifts,” *Eur. Phys. J. C* **77**, 896 (2017).
- [17] J. C. Berengut, C. Delaunay, A. Geddes, and Y. Soreq, “Generalized King linearity and new physics searches with isotope shifts,” *Phys. Rev. Res.* **2**, 043444 (2020).
- [18] F. Gebert, Y. Wan, F. Wolf, C. N. Angstmann, J. C. Berengut, and P. O. Schmidt, “Precision Isotope Shift Measurements in Calcium Ions Using Quantum Logic Detection Schemes,” *Physical Review Letters* **115**, 053003 (2015).
- [19] B. Braverman, A. Kawasaki, E. Pedrozo-Peñafiel, S. Colombo, C. Shu, Z. Li, E. Mendez, M. Yamoah, L. Salvi, D. Akamatsu, Y. Xiao, and V. Vuletić, “Near-

- unitary spin squeezing in  $^{171}\text{Yb}$ ,” *Phys. Rev. Lett.* **122**, 223203 (2019).
- [20] T. Manovitz, R. Shaniv, Y. Shapira, R. Ozeri, and N. Akerman, “Precision measurement of atomic isotope shifts using a two-isotope entangled state,” *Phys. Rev. Lett.* **123**, 203001 (2019).
- [21] I. Counts, J. Hur, D. P. L. Aude Craik, H. Jeon, C. Leung, J. C. Berengut, A. Geddes, A. Kawasaki, W. Jhe, and V. Vuletić, “Evidence for nonlinear isotope shift in  $\text{Yb}^+$  search for new boson,” *Phys. Rev. Lett.* **125**, 123002 (2020).
- [22] A. Papoulia, B. G. Carlsson, and J. Ekman, “Effect of realistic nuclear charge distributions on isotope shifts and progress towards the extraction of higher-order nuclear radial moments,” *Phys. Rev. A* **94**, 042502 (2016).
- [23] J. Ekman, P. Jönsson, M. Godefroid, C. Nazé, G. Gaigalas, and J. Bieroń, “ris 4: A program for relativistic isotope shift calculations,” *Comput. Phys. Commun.* **235**, 433 – 446 (2019).
- [24] P.-G. Reinhard, W. Nazarewicz, and R. F. Garcia Ruiz, “Beyond the charge radius: The information content of the fourth radial moment,” *Phys. Rev. C* **101**, 021301(R) (2020).
- [25] S. O. Allehabi, V. A. Dzuba, V. V. Flambaum, and A. V. Afanasjev, “Nuclear deformation as a source of the non-linearity of King plot in the  $\text{Yb}^+$  ion,” (2020), [arXiv:2012.04043 \[physics.atom-ph\]](https://arxiv.org/abs/2012.04043).
- [26] J. L. Friar and J. W. Negele, “Theoretical and experimental determination of nuclear charge distributions,” *Adv. Nucl. Phys.* **8**, 219–376 (1975).
- [27] J. Friedrich and P.-G. Reinhard, “Skyrme-force parametrization: Least-squares fit to nuclear ground-state properties,” *Phys. Rev. C* **33**, 335–351 (1986).
- [28] T. de Forest Jr. and J. Walecka, “Electron scattering and nuclear structure,” *Adv. Phys.* **15**, 1–109 (1966).
- [29] W. Bertozzi, J. Friar, J. Heisenberg, and J. Negele, “Contributions of neutrons to elastic electron scattering from nuclei,” *Phys. Lett. B* **41**, 408 – 414 (1972).
- [30] J. Friar, “Relativistic corrections to electron scattering by  $2\text{H}$ ,  $3\text{He}$ , and  $4\text{He}$ ,” *Ann. Phys. (N.Y.)* **81**, 332 – 363 (1973).
- [31] J. Martorell and D. W. L. Sprung, “Contribution of the electromagnetic spin-orbit interaction to the isotopic charge density differences in lead,” *Z. Phys. A* **298**, 153–157 (1980).
- [32] J. L. Friar, J. Martorell, and D. W. L. Sprung, “Nuclear sizes and the isotope shift,” *Phys. Rev. A* **56**, 4579–4586 (1997).
- [33] C. Lorcé, “Charge distributions of moving nucleons,” *Phys. Rev. Lett.* **125** (2020), [10.1103/PhysRevLett.125.232002](https://arxiv.org/abs/10.1103/PhysRevLett.125.232002).
- [34] G. Hagen, A. Ekström, C. Forssén, G. R. Jansen, W. Nazarewicz, T. Papenbrock, K. A. Wendt, S. Bacca, N. Barnea, B. Carlsson, C. Drischler, K. Hebeler, M. Hjorth-Jensen, M. Miorelli, G. Orlandini, A. Schwenk, and J. Simonis, “Neutron and weak-charge distributions of the  $^{48}\text{Ca}$  nucleus,” *Nat. Phys.* **12**, 186 (2016).
- [35] M. Hoferichter, J. Menéndez, and A. Schwenk, “Coherent elastic neutrino-nucleus scattering: Eft analysis and nuclear responses,” *Phys. Rev. D* **102**, 074018 (2020).
- [36] P. G. Reinhard, “The relativistic mean-field description of nuclei and nuclear dynamics,” *Rep. Prog. Phys.* **52**, 439–514 (1989).
- [37] M. Bender, P.-H. Heenen, and P.-G. Reinhard, “Self-consistent mean-field models for nuclear structure,” *Rev. Mod. Phys.* **75**, 121–180 (2003).
- [38] P.-G. Reinhard, J. Piekarewicz, W. Nazarewicz, B. K. Agrawal, N. Paar, and X. Roca-Maza, “Information content of the weak-charge form factor,” *Phys. Rev. C* **88**, 034325 (2013).
- [39] T. Liang, J. Liu, Z. Ren, C. Xu, and S. Wang, “Elastic electron scattering form factors of deformed exotic  $\text{Xe}$  isotopes,” *Phys. Rev. C* **98**, 044310 (2018).
- [40] S. O. Allehabi, V. A. Dzuba, V. V. Flambaum, A. V. Afanasjev, and S. E. Agbemava, “Using isotope shift for testing nuclear theory: The case of nobelium isotopes,” *Phys. Rev. C* **102**, 024326 (2020).
- [41] A. Ong, J. C. Berengut, and V. V. Flambaum, “Effect of spin-orbit nuclear charge density corrections due to the anomalous magnetic moment on halo nuclei,” *Phys. Rev. C* **82**, 014320 (2010).
- [42] C. J. Horowitz and J. Piekarewicz, “Impact of spin-orbit currents on the electroweak skin of neutron-rich nuclei,” *Phys. Rev. C* **86**, 045503 (2012).
- [43] H. Kurasawa and T. Suzuki, “The  $n$ th-order moment of the nuclear charge density and contribution from the neutrons,” *Prog. Theor. Exp. Phys.* **2019** (2019), [10.1093/ptep/ptz121](https://arxiv.org/abs/10.1093/ptep/ptz121).
- [44] H. Kurasawa and T. Suzuki, “Effects of the neutron spin-orbit density on the nuclear charge density in relativistic models,” *Phys. Rev. C* **62**, 054303 (2000).
- [45] J. D. Bjorken and S. D. Drell, *Relativistic Quantum Mechanics* (McGraw–Hill, New York, 1964).
- [46] K. Schmid and P.-G. Reinhard, “Center-of-mass projection of Skyrme-Hartree-Fock densities,” *Nucl. Phys. A* **530**, 283–302 (1991).
- [47] B. Mihaila and J. H. Heisenberg, “Center-of-mass corrections reexamined: A many-body expansion approach,” *Phys. Rev. C* **60**, 054303 (1999).
- [48] G. Hagen, T. Papenbrock, and D. J. Dean, “Solution of the center-of-mass problem in nuclear structure calculations,” *Phys. Rev. Lett.* **103**, 062503 (2009).
- [49] P. Klüpfel, P.-G. Reinhard, T. J. Bürvenich, and J. A. Maruhn, “Variations on a theme by Skyrme,” *Phys. Rev. C* **79**, 034310 (2009).
- [50] P.-G. Reinhard and W. Nazarewicz, “Toward a global description of nuclear charge radii: Exploring the Fayans energy density functional,” *Phys. Rev. C* **95**, 064328 (2017).
- [51] P.-G. Reinhard, B. Schuetrumpf, and J. Maruhn, “The axial Hartree-Fock + BCS code SkyAx,” *Comp. Phys. Comm.* **258**, 107603 (2021).
- [52] S. J. Krieger, P. Bonche, H. Flocard, P. Quentin, and M. S. Weiss, “An improved pairing interaction for mean-field calculations using skyrme potentials,” *Nucl. Phys. A* **517**, 275 (1990).
- [53] M. Bender, K. Rutz, P.-G. Reinhard, and J. A. Maruhn, “Pairing gaps from nuclear mean-field models,” *Eur. Phys. J. A* **8** (2000), [10.1007/s10050-000-4504-z](https://arxiv.org/abs/10.1007/s10050-000-4504-z).
- [54] J. Dobaczewski, H. Flocard, and J. Treiner, “Hartree-Fock-Bogolyubov description of nuclei near the neutron-drip line,” *Nucl. Phys. A* **422**, 103 – 139 (1984).
- [55] J. Dobaczewski, W. Nazarewicz, T. R. Werner, J. F. Berger, C. R. Chinn, and J. Dechargé, “Mean-field description of ground-state properties of drip-line nuclei: Pairing and continuum effects,” *Phys. Rev. C* **53**, 2809–2840 (1996).
- [56] G. Simon, C. Schmitt, F. Borkowski, and V. Walther,

- “Absolute electron-proton cross sections at low momentum transfer measured with a high pressure gas target system,” *Nucl. Phys. A* **333**, 381 – 391 (1980).
- [57] V.H. Walther private communication, (1986).
- [58] H. Emrich, G. Fricke, G. Mallot, H. Miska, H.-G. Sieberling, J. Cavedon, B. Frois, and D. Goutte, “Radial distribution of nucleons in the isotopes  $^{48,40}\text{Ca}$ ,” *Nucl. Phys. A* **396**, 401 – 408 (1983).
- [59] A. Grinin, A. Matveev, D. C. Yost, L. Maisenbacher, V. Wirthl, R. Pohl, T. W. Hänsch, and T. Udem, “Two-photon frequency comb spectroscopy of atomic hydrogen,” *Science* **370**, 1061–1066 (2020).
- [60] M. Tanabashi *et al.* (Particle Data Group), “Review of particle physics,” *Phys. Rev. D* **98**, 030001 (2018).
- [61] T. D. Goodacre *et al.*, “Laser spectroscopy of neutron-rich  $^{207,208}\text{Hg}$  isotopes: Illuminating the kink and odd-even staggering in charge radii across the  $N = 126$  shell closure,” (2020), [arXiv:2012.13802 \[nucl-ex\]](https://arxiv.org/abs/2012.13802).